Phonon dispersion effects and the thermal conductivity reduction in GaAs/AlAs superlattices

W. E. Bies, R. J. Radtke, and H. Ehrenreich

Citation: Journal of Applied Physics **88**, 1498 (2000); doi: 10.1063/1.373845
View online: https://doi.org/10.1063/1.373845
View Table of Contents: http://aip.scitation.org/toc/jap/88/3
Published by the American Institute of Physics

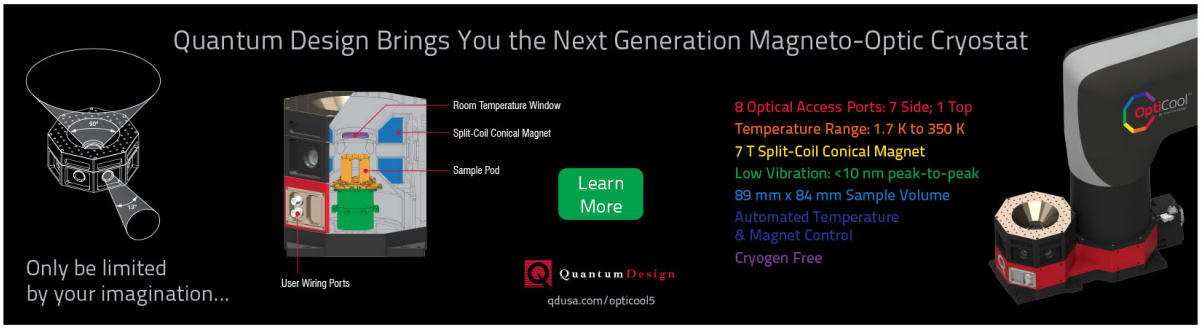

Phonon dispersion effects and the thermal conductivity reduction in GaAs/AlAs superlattices

W. E. Bies, R. J. Radtke,[a] and H. Ehrenreich[b]
Department of Physics and Division of Engineering and Applied Sciences, Harvard University, Cambridge, Massachusetts 02138

(Received 10 January 2000; accepted for publication 28 April 2000)

The experimentally observed order-of-magnitude reduction in the thermal conductivity along the growth axis of $(GaAs)_n/(AlAs)_n$ (or $n\times n$) superlattices is investigated theoretically for (2×2), (3×3) and (6×6) structures using an accurate model of the lattice dynamics. The modification of the phonon dispersion relation due to the superlattice geometry leads to flattening of the phonon branches and hence to lower phonon velocities. This effect is shown to account for a factor-of-three reduction in the thermal conductivity with respect to bulk GaAs along the growth direction; the remainder is attributable to a reduction in the phonon lifetime. The dispersion-related reduction is relatively insensitive to temperature ($100<T<300$ K) and n. The phonon lifetime reduction is largest for the 2×2 structures and consistent with greater interface scattering. The thermal conductivity reduction is shown to be appreciably more sensitive to GaAs/AlAs force constant differences than to those associated with molecular masses. © *2000 American Institute of Physics.* [S0021-8979(00)06415-X]

I. INTRODUCTION

Superlattice structures have been proposed to be materials with a high thermoelectric figure of merit *ZT*, for both in-plane[1] and cross-plane[2,3] current flow. In the latter case, the improvement in thermoelectric performance is attributable to a reduced lattice thermal conductivity[2–4] rather than to a higher electronic conductivity. Experimentally, a factor-of-ten reduction in the component of lattice thermal conductivity along the growth axis, $\kappa_{l,zz}$, is observed in GaAs/AlAs[5,6] and Bi_2Te_3/Sb_2Te_3[7,8] superlattices (SLs). Theoretically, the thermal conductivity of Si/Ge SLs has been studied previously by Hyldgaard and Mahan[9] and by Chen.[10] Within the context of a very simplified model of the phonon dynamics, the calculations of Ref. 9 were able to reproduce the factor-of-ten reduction in the thermal conductivity along the growth direction. By contrast, Chen's[10] extensive work focused on the role of thermal boundary resistance. The present article investigates the reduction associated with SL induced changes of the phonon dispersion based on a realistic, computationally intensive treatment of the phonon spectra and dynamics.

The origin of the observed reduction in thermal conductivity may be explained qualitatively as follows. First, we note that in the experimental work of Capinski and Maris[5] and Capinski *et al.*[6] on $(GaAs)_n/(AlAs)_n$ SLs for n up to 40, the phonon mean free path inferred from the thermal conductivity, heat capacity, and Debye velocity is greater than 370 Å at all temperatures for which measurements exist, always large compared to the size of the SL unit cell 5.66 Å. Thus, the phonon transport lies in a regime where the SL phonon dispersion relation and lifetime, and not those of the bulk constituents, determine the thermal conductivity. According to the expression for the thermal conductivity derived from the phonon Boltzmann equation in the relaxation-time approximation [see Eq. (6)], the thermal conductivity depends on: (1) a quantity representing the contribution of the SL phonon dispersion relation, and (2) the lifetime τ, which contains phonon–phonon, interface and defect scattering effects. We shall focus only on item (1), whose effect can be computed within our realistic, albeit complicated, lattice-dynamical model. The effect of the SL geometry is to introduce anticrossings and new gaps in the phonon dispersion relation, when the magnitude of the phonon wave vector along the growth direction equals an integer multiple of π/d, where d is the period of the SL along the growth direction. The consequent flattening of the phonon branches near the Brillouin zone edge leads to a lowering of phonon velocities in the growth direction, and hence a reduction in thermal conductivity.

We describe in Sec. II the lattice-dynamical model for the SL, which is a generalization of the 11-parameter rigid-ion model of Kunc.[11,12] It incorporates short-range interactions to next nearest neighbors and the long-range Coulomb interaction. The construction of the SL dynamical matrix is outlined in Sec. II and in the Appendix.

The formalism is applied to a $(GaAs)_3/(AlAs)_3$ SL in Sec. III. The phonon dispersion relation will be seen to display the flattening expected for a SL. Critical points, especially at the high-symmetry points Γ, X and Z, produce sharp peaks in the density of states in the SL. Miniband formation and anticrossings in the SL phonon dispersion relation lead to a threefold reduction, relative to bulk, in the contribution of the phonon dispersion relation to the thermal conductivity along the growth direction. The present results contrast with those of Hyldgaard and Mahan,[9] who found that in their

[a]Present address: Schlumberger, Sugar Land Product Center, 110 Schlumberger Dr., MD110-4, Sugar Land, TX 77478.
[b]Author to whom correspondence should be addressed; electronic mail: ehrenrei@deas.harvard.edu

simplified model the order-of-magnitude reduction of κ_{zz}/τ was attributable to effects related to the SL dispersion relation alone. In our more realistic treatment of the SL dynamics, a significant threefold reduction in the lifetime is also needed to explain the experimental reduction in κ_{zz} by a factor of 10. Finally, the sensitivity of the decrease in κ_{zz} to differences in masses or force constants between the GaAs and AlAs layers is investigated; differences in the force constants are found to play a markedly greater role in the reduction of κ_{zz} than differences in mass.

Section IV is devoted to discussion and conclusions which are broadened by examining the dependence of our results on the period n of the $(GaAs)_n/(AlAs)_n$ SL for $n=2$, 3 and 6. These results permit some discussion of interface effects on the phonon lifetime and a more detailed comparison of the present work with that of Refs. 9 and 10. The reduction in the contribution of the phonon dispersion relation to the thermal conductivity of the SL relative to bulk is computed, and found to be approximately independent of n for the small values considered here. The lifetime for both the SL and bulk was determined using the experimental thermal conductivities of the SL and of bulk GaAs of Capinski *et al.*[6] The lifetimes are found to be smaller for the 2×2 SL and larger and roughly equal for the 3×3 and 6×6 SLs, consistent with the presence of greater interface scattering in the 2×2 SLs.

II. FORMALISM

The lattice dynamics can be treated realistically via the 11-parameter rigid-ion model of Kunc,[11,12] which has been successfully applied to zinc-blende–structure compounds. Consider $(GaAs)_3/(AlAs)_3$. In the SL unit cell, consisting of a layer of GaAs above a layer of AlAs in the growth direction, there will be three pairs of GaAs followed by three pairs of AlAs, or three Ga, three Al, and six As atoms in all, which may be indexed by $\kappa=1,...,12$. Letting $u_\alpha(l\kappa)$ denote the displacement in the direction $\alpha=x,y,z$ of the κth atom in the lth unit cell, plane-wave solutions of the form

$$u_\alpha(l\kappa)=M_\kappa^{-1/2}e^{i(\mathbf{k}\cdot\mathbf{x}(l\kappa)-\omega_j(\mathbf{k})t)}w_\alpha(\kappa|\mathbf{k}j) \tag{1}$$

are assumed, where $\mathbf{x}(l\kappa)$ is the equilibrium position of the κth atom in the lth unit cell, and $w_\alpha(\kappa|\mathbf{k}j)$ satisfies the secular equation

$$\omega_j(\mathbf{k})^2 w_\alpha(\kappa|\mathbf{k}j)=\sum_{\beta\kappa'} C_{\alpha\beta}(\kappa\kappa'|\mathbf{k})w_\beta(\kappa'|\mathbf{k}j). \tag{2}$$

The dynamical matrix $\underline{C}$ reflects the interatomic force constants of the crystal. In the present rigid-ion model, the interatomic forces are divided into: (1) short-range forces extending to second nearest neighbors, and (2) the long-range Coulomb interaction. Accordingly, the dynamical matrix may be written

$$\underline{C}=\underline{C}_{\rm sr}+\underline{C}_{\rm Coul}. \tag{3}$$

As a result of symmetry of the zinc-blende structure, the short-range forces to second nearest neighbors may be described by 10 parameters for each material.[12] For nearest and next nearest neighbor interactions in the SL unit cell, we employ the force constants determined for the constituent bulk materials separately, rotated by the appropriate point-group operation.[13] Bulk GaAs and AlAs parameters are taken from the literature.[14,15] In the SL, bulk parameters are used within each layer. For the interface atoms and Ga–Al bonds crossing the interface, we employ the average of the bulk parameters following Ren *et al.*[15] For the Coulomb interaction, the atoms are treated as point charges. The Madelung sum and its derivatives are computed using the usual Ewald transformation,[16] which has been generalized here for SLs. This is accomplished by separating the sum over the spatial index l into a sum over layers normal to the growth direction $l_\parallel$, and a sum along the growth axis l_z. A two-dimensional Ewald transformation is performed in each layer; these results are then summed over l_z. The resulting expressions for the function $\phi(\mathbf{k},\mathbf{r})$ and its derivatives (see the Appendix) are similar to those that arise in the usual three-dimensional Ewald procedure; however, the definite integrals differ and must be performed numerically. Detailed expressions for the Coulomb term are given in the Appendix.

The phonon Boltzmann equation in the relaxation-time approximation leads to the following expression for the lattice thermal conductivity:

$$\kappa_{ij}=\int\frac{d^3q}{(2\pi)^3}\sum_\alpha \hbar\omega_{\mathbf{q}}^{(\alpha)}\frac{\partial\omega_{\mathbf{q}}^{(\alpha)}}{\partial q_i}\frac{\partial\omega_{\mathbf{q}}^{(\alpha)}}{\partial q_j}\times\frac{dn(\omega_{\mathbf{q}}^{(\alpha)})}{dT}\tau_{\rm ph}(\omega_{\mathbf{q}}^{(\alpha)},T), \tag{4}$$

where $n(\omega_{\mathbf{q}}^{(\alpha)})$ is the distribution function of the phonons, the sum is over branches α, and $\tau_{\rm ph}(\omega_{\mathbf{q}}^{(\alpha)},T)$ is the lifetime. Equation (4) can be written in terms of

$$\Sigma_{ij}(\omega)=\int\frac{d^3q}{(2\pi)^3}\sum_\alpha \hbar\omega_{\mathbf{q}}^{(\alpha)}\frac{\partial\omega_{\mathbf{q}}^{(\alpha)}}{\partial q_i}\frac{\partial\omega_{\mathbf{q}}^{(\alpha)}}{\partial q_j}\delta(\omega-\omega_{\mathbf{q}}^{(\alpha)}) \tag{5}$$

as

$$\kappa_{ij}=\int d\omega(dn(\omega)/dT)\Sigma_{ij}(\omega)\tau_{\rm ph}(\omega,T). \tag{6}$$

This article will focus on the SL effects on the dispersion relation contained in $\Sigma_{ij}(\omega)$. Relaxation-time effects associated, for example, with scattering from interfaces, defects, umklapp processes, etc. are not considered explicitly. However, the results will be used to infer some of their properties.

III. $(GaAs)_3/(AlAs)_3$ SUPERLATTICES

We focus first on the $(GaAs)_3/(AlAs)_3$ SL studied experimentally by Capinski and Maris.[5] Using a picosecond pump-and-probe technique, they observed an order-of-magnitude reduction in the thermal conductivity along the growth direction κ_{zz} relative to bulk GaAs. The dispersion relation along the ΓX and ΓZ directions, which was generated numerically according to the method described in Sec. II, is shown in Fig. 1. The significance of the labeled features will be explained in the discussion of Fig. 2. Because the SL unit cell contains three unit cells each of bulk GaAs and bulk AlAs, respectively, arranged along the growth axis, the edge

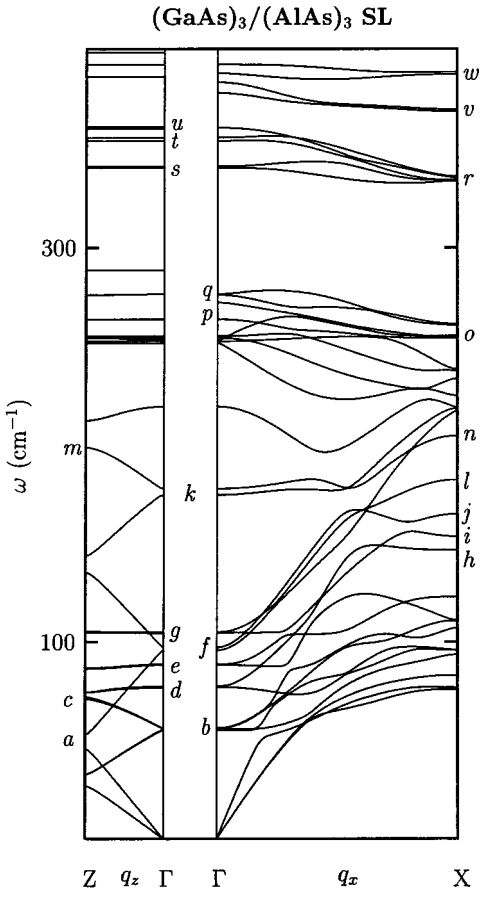

FIG. 1. $(GaAs)_3/(AlAs)_3$ SL dispersion relation along the $\Gamma X = (2\pi/a_0,0,0)$ and $\Gamma Z = (0,0,\pi/3a_0)$ directions; a_0 is the conventional GaAs unit cell size. The labels $a-w$ are defined in Fig. 2.

of the SL Brillouin zone in the growth direction Z is one-sixth as far from the center as it is in the in-plane directions X and Y. As a result each of the six branches in the bulk material is folded back six times along ΓZ, which is most easily seen for the longitudinal acoustic mode in Fig. 1. Bulk GaAs and bulk AlAs optical modes have no frequencies in

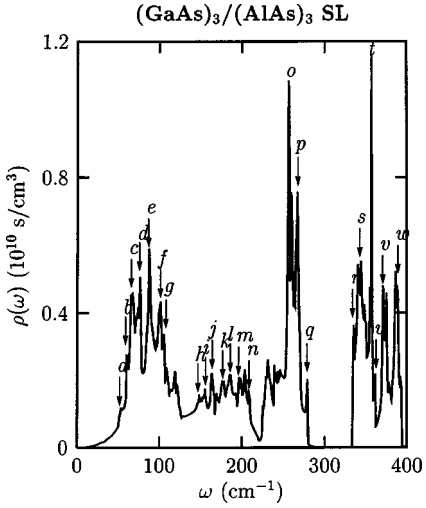

FIG. 2. Phonon density of states for the $(GaAs)_3/(AlAs)_3$ SL, with labeled critical points identified with features in the dispersion relation in Fig. 1.

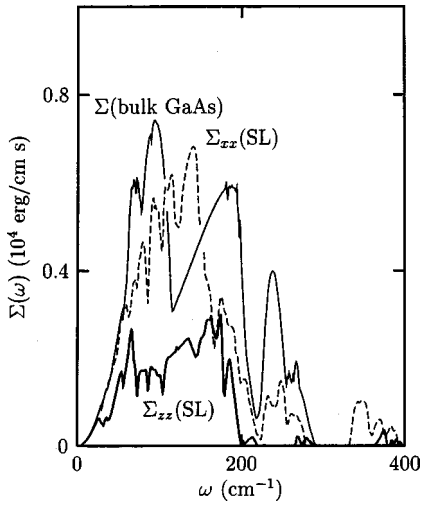

FIG. 3. The transport quantities $\Sigma_{xx}(\omega)$ and $\Sigma_{zz}(\omega)$, defined by Eq. (5) for bulk GaAs (solid line) and the $(GaAs)_3/(AlAs)_3$ SL (dashed and bold lines).

common, and are therefore localized. This leads to: (1) flat SL dispersion in optical modes and (2) localization of AlAs optical modes to the AlAs layer. The GaAs optical modes are not localized, since they overlap with the acoustic modes as shown in Fig. 1 along ΓX. Due to the nonanalyticity of C_{Coul} as $q\to 0$ in the SL, $\omega(|q|\to 0)$ differ along ΓX and ΓZ (see Ref. 15).

The density of states $\rho(\omega)$ versus frequency, computed using the tetrahedral integration method as presented in MacDonald *et al.*,[17] is given in Fig. 2. Note the transverse–acoustic features around $\omega = 80-100\,\mathrm{cm}^{-1}$, the longitudinal–acoustic features around 150–200 cm^{-1}, the GaAs optical feature at 220–260 cm^{-1}, and, separated in frequency at higher frequencies, the AlAs optical feature at 330–400 cm^{-1}. Band gaps at the zone edge and anticrossings in Fig. 1 yield critical points which, depending on the amount of $\mathbf{q}$ space at those frequencies, produce sharp structure in the density of states. As shown in Fig. 2, this structure in the density of states can be correlated with features in the dispersion relation, usually at the Γ (for folded-back bands), X, and Z points. The structures at Γ, X, and Z labeled in Fig. 2 are identified with the corresponding features in Fig. 1. The strength of each feature depends on the integral of $\delta(\omega - \omega_{\mathbf{q}}^{(\alpha)})$ (cf. Fig. 2) at that frequency, which will be large if $|\mathbf{v}|$ is small. Surprisingly, most of the peaks in the density of states (DOS) appear to be associated with the critical points at Γ, X, and Z. No such fine structure in the density of states exists in bulk GaAs or bulk AlAs, as may be seen for instance in Patel *et al.*[14] for GaAs. (The DOS for AlAs is not available in the literature, but our calculations confirmed the absence of fine structure for AlAs as well.)

Figure 3 shows the results for $\Sigma(\omega)$, as defined in Eq. (5), for bulk GaAs and the SL. Note that optical modes do not contribute appreciably to $\Sigma_{zz}(\omega)$ in the SL, an effect of localization in the AlAs layers: flat dispersion leads to a vanishing of $\partial\omega_{\mathbf{q}}^{(\alpha)}/\partial q_z$. The fine structure in the DOS is also correlated with that in $\Sigma(\omega)$: peaks in the DOS$\propto\int dS/|\mathbf{v}|$ become dips in $\Sigma\propto\int v^2 dS/|\mathbf{v}|$. (Here, S denotes the surface of constant frequency ω in the Brillouin zone; it consists not

only of the surface containing the critical point, but also possibly of other surfaces at the same ω elsewhere in the zone.) Acoustic modes in the SL contribute less than they would in bulk because of the band-gap and anticrossing-induced reduction in v^2. This leads to a threefold reduction in κ_{ℓ}/τ at 300 K, determined here either by integrating Eq. (4) directly on a $60\times60\times20$ grid covering an irreducible wedge of the Brillouin zone, or by integrating Eq. (6). Experimentally, Capinski and Maris[5] found a tenfold reduction factor for $(GaAs)_3/(AlAs)_3$. The full reduction factor is a product of the reduction due to Σ and that due to τ. Assuming τ to be constant at any given temperature, it can be found by requiring equality in Eqs. (4) or (6) to the experimental value for the thermal conductivity in bulk or SL, respectively, if the appropriate dispersion relation is used in computing κ_{zz}/τ. The lifetime in bulk versus lifetime in SL, as well as the layer-width dependence of the results, will be discussed below. Finally, we note that $\Sigma_{zz}<\Sigma_{xx}$ in the SL for the simple physical reason that band flattening along the q_z direction affects $\partial\omega/\partial q_z$ more than $\partial\omega/\partial q_x$.

The reduction in thermal conductivity due to Σ can be understood by means of an easily visualized picture in $\mathbf{q}$ space. In bulk, the quantity $q_x\Sigma_\alpha[dn(\omega_{\mathbf{q}}^{(\alpha)})/dT]\omega_{\mathbf{q}}^{(\alpha)}(v_{\mathbf{q},z}^{(\alpha)})^2$ represents the contribution of the phonon dispersion relation in Eq. (4). In a range Δq_x of the integrand it is weighted by q_x because, with the dispersion relation being rotationally symmetric in the (q_x,q_y) plane, we may integrate around the circle of radius q_x to yield a properly weighted function of q_x and q_z alone. The quantity is plotted in Figs. 4(a), 4(b), and 4(c) (bold line) together with the corresponding values for GaAs (light solid line) as a function of q_z for three values of q_x. The SL contribution is reasonably localized in q_z. To gain physical insight, we replace it by the dashed rectangles (of equal area). This approximate localization is related to the reduction at $q_z\approx0$ and π/d due to miniband formation (that is, flattening of ω vs q) and has dips from anticrossings, as in Fig. 4(a), for instance. The dependence on q_x can then the summarized by the density plot in Fig. 4(d), comparing the SL on the left to bulk GaAs on the right. For GaAs the equivalent rectangles extend over the entire range of q_z because there is no localization due to band flattening at the zone edge as in the case of the SL. The shading indicates the weight of each increment Δq_x. We find that points around $q_x=\pi/d$ and at the zone edge $(q_x=6\pi/d)$ contribute most to heat transport. The latter is due to the effect of the weighting by q_x in the annular integration. In addition, this weighting causes the contribution from points near the origin to be very small. A simple numerical estimate leads to a reduction in Σ by 34%, which is to be compared to 36% in the exact calculation.

Finally, we discuss the sensitivity of variation of the mass differences, force constants, and effective ionic charge e^* between layers on the thermal conductivity. This manifests itself through variations of the zone edge gap and hence the group velocity. This effect has been studied by interpolating e^*, the force constants K, and cation mass M between their AlAs and their GaAs values in the GaAs layer. Here K refers collectively to the 10 Kunc parameters describing interatomic forces. Explicitly, starting from $(AlAs)_6$ we: (i)

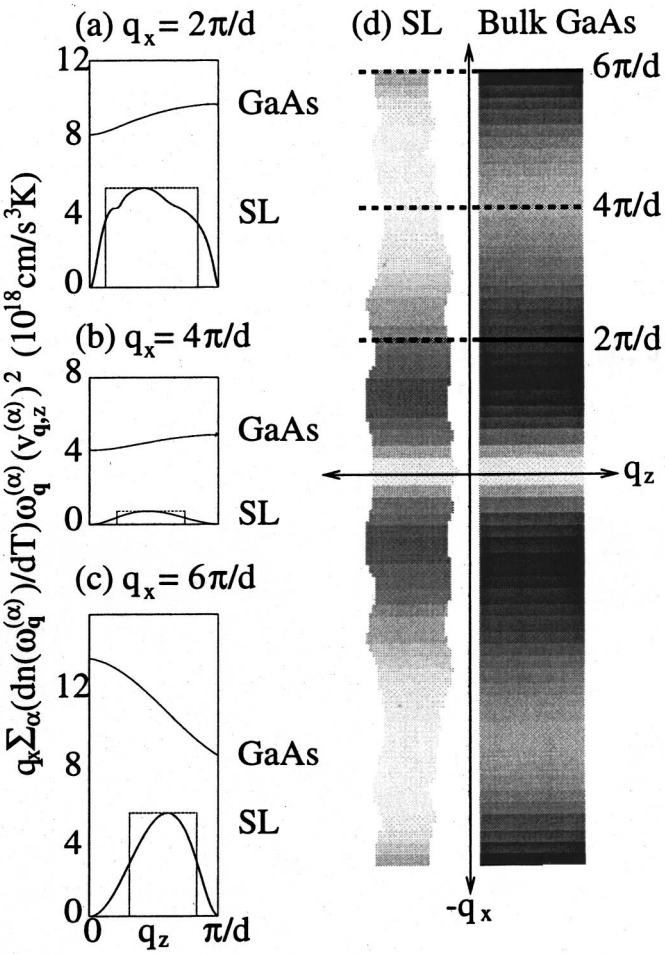

FIG. 4. The transport quantity $q_x(dn/dT)\Sigma_\alpha\omega_{\mathbf{q}}^{(\alpha)}(v_{\mathbf{q},z}^{(\alpha)})^2$ for $0\leq q_z\leq\pi/d$ at fixed q_x, for (a) $q_x=2\pi/d$, (b) $q_x=4\pi/d$, and (c) $q_x=6\pi/d$; solid line: bulk GaAs; bold line: $(GaAs)_3/(AlAs)_3$ SL. (d) Density plot in the (q_x,q_z) plane whose shading indicates the weight of each increment Δq_x along q_x to the value of this transport quantity for the $(GaAs)_3/(AlAs)_3$ SL and bulk GaAs.

vary e^{*2} and M linearly in three neighboring AlAs positions to make a $(AlAs)_3/(GaAs)_3$ SL. In the case of the masses we put $M=(1-\alpha)M_{\mathrm{Al}}+\alpha M_{\mathrm{Ga}}$ so that at $\alpha=0$ and 1 they correspond respectively to Al and Ga; (ii) very e^{*2} and force constants K linearly in α in the same way; and (iii) vary e^{*2}, and M and K linearly in α. The results are given in Fig. 5. The thermal conductivity is seen to be far more sensitive to the variation of force constants than the variation in mass. The variation of the force constants alone produces band flattening which reduces the thermal conductivity by about 60%. The additional flattening due to changing masses leads to only a few percent additional reduction.

IV. DISCUSSION AND CONCLUSIONS

Before turning to the final results, we emphasize again that this article is primarily concerned with the effects of superlattice induced changes of the phonon dispersion on the lattice thermal conductivity. Since a SL is a perfect crystal, the ideal structures under discussion here automatically include the coherent effects associated with perfect interfaces. The importance of including such effects was first pointed

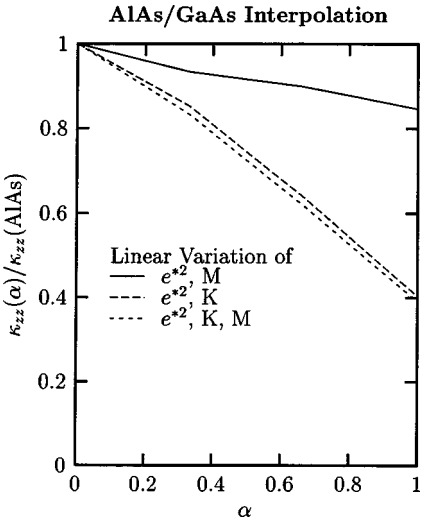

FIG. 5. Dependence of κ_{zz} as e^{*2} and the mass M (solid line), the spring constants K (long-dashed line) and both M and K (short-dashed line) are interpolated between their AlAs ($\alpha=0$) and GaAs values ($\alpha=1$) for the atoms in three contiguous layers in what is initially $(AlAS)_6$ at $\alpha=0$.

out by Hyldgaard and Mahan[9] in connection with a simple, highly idealized model for Si/Ge SLs. Extensive work by Chen[10] focused on diffuse interface scattering of phonons. His model assumes SL layers sufficiently thick that the phonon spectrum in each layer corresponds to that of the bulk. A mixture of spectral and diffuse interface processes is found to be sufficient to explain the observed experimental reduction of the SL thermal conductivity relative to bulk. As already pointed out, the more realistically modeled results of the present article for κ_l/τ lead to a threefold reduction without any assumptions about the SL phonon scattering mechanisms. Our results must therefore be viewed as complementary to those of Chen.[10] Taken together, they suggest that a combination of phonon spectral changes and imperfect interfaces can account adequately for the observed reduction.

The present calculations permit some statements concerning lifetime effects from the dependence of the SL results on layer width. This dependence was studied numerically for 2×2, 3×3 and 6×6 GaAs/AlAsSLs. The results for

$$\bar{\Sigma}_{zz}\equiv\kappa_{zz}/\tau=\int\frac{d^3q}{(2\pi)^3}\sum_{\alpha}\hbar\omega_{\mathbf{q}}^{(\alpha)}\frac{\partial\omega_{\mathbf{q}}^{(\alpha)}}{\partial q_i}\frac{\partial\omega_{\mathbf{q}}^{(\alpha)}}{\partial q_j}\frac{dn(\omega_{\mathbf{q}}^{(\alpha)})}{dT} \tag{7}$$

are given in Table I. τ is assumed constant. Given an experimental value for κ_{zz} and the calculated value of $\bar{\Sigma}_{zz}$, the lifetimes listed in Table I are found as $\tau=\kappa_{zz}/\bar{\Sigma}_{zz}$; only the lifetime itself is given in Table I and not $\bar{\Sigma}_{zz}$, but the ratios $\bar{\Sigma}_{zz}(\mathrm{SL})/\bar{\Sigma}_{zz}$ (bulk) are listed because we are interested in

$$\frac{\tau_{\mathrm{SL}}}{\tau_{\mathrm{bulk}}}=\frac{\bar{\Sigma}_{zz}(\mathrm{bulk})}{\bar{\Sigma}_{zz}(\mathrm{SL})}\frac{\kappa_{zz}^{\mathrm{SL}}(\mathrm{expt})}{\kappa_{zz}^{\mathrm{bulk}}(\mathrm{expt})}. \tag{8}$$

The SL $\bar{\Sigma}_{zz}$ is found to have a value about 40% of the bulk, and to be relatively insensitive to the SL period and temperature. For larger SL periods, there is more folding back, but this is compensated by the smaller size of the gaps at the zone edge, which is found in the computed ΓZ dispersion relations to scale inversely with the SL period. The two effects balance, resulting in an approximately constant reduction factor. The phonon lifetimes for the 2×2, 3×3, and 6×6 SLs are also given in Table I. The bulk lifetime is the same to within 2% for the different SL periods, as it must be. The ratio of SL to bulk lifetimes is significantly smaller for the 2×2 SLs at each temperature, while it is larger and roughly the same for the 3×3 and 6×6 SLs. Thus, the reduction in thermal conductivity may be divided into a dispersive part which is insensitive to $n\times n$ and a scattering part which is sensitive to interface scattering. The results for the 2×2 SL are possibly associated with the experimental difficulties associated with achieving sufficiently perfect interfaces for small n.

TABLE I. Reduction in $\bar{\Sigma}_{zz}=\kappa_{zz}/\tau$ relative to bulk GaAs for 2×2, 3×3, and 6×6 SLs at $T=100$, 200, and 300 K, and SL phonon lifetimes deduced from Eq. (8) for the 2×2, 3×3, and 6×6 SLs at each temperature.

SL	Experimental $\kappa_{zz}^{\mathrm{SL}}$ (W/cm K)[a]	Theoretical $\frac{\bar{\Sigma}_{zz}(\mathrm{SL})}{\bar{\Sigma}_{zz}(\mathrm{bulk})}$	τ_{bulk} (ps)	τ_{SL} (ps)	$\tau_{\mathrm{SL}}/\tau_{\mathrm{bulk}}$
		$T=300$ K, $\kappa_{zz}^{\mathrm{bulk}}=0.45$ W/cm K[b]			
2×2	0.040	0.38	36.8	8.7	0.24
3×3	0.068	0.36	37.2	15	0.42
6×6	0.053	0.34	37.2	13	0.35
		$T=200$ K, $\kappa_{zz}^{\mathrm{bulk}}=0.64$ W/cm K[b]			
2×2	0.055	0.38	55.2	12	0.22
3×3	0.090	0.39	56.1	20	0.36
6×6	0.072	0.35	55.7	18	0.32
		$T=100$ K, $\kappa_{zz}^{\mathrm{bulk}}=2.0$ W/cm K[b]			
2×2	0.065	0.40	222	18	0.08
3×3	0.110	0.42	227	30	0.14
6×6	0.096	0.37	222	29	0.13

[a]Experimental values for GaAs/AlAs reported by Ref. 6.
[b]Experimental value for GaAs listed in Ref. 5.

The present calculations imply: (1) that a similar reduction in the contribution of the SL phonon dispersion relation to transport in the growth direction, and perhaps in κ_{zz} itself, may be expected in any SL with similar mass or force-constant differences between layers. (2) If the lifetime is reduced in SLs by increased umklapp scattering, as suggested by Ren and Dow,[13] then the present calculations give an upper bound on the SL κ_{zz} and a lower bound on the increase in ZT in a SL relative to bulk.

ACKNOWLEDGMENTS

The authors wish to thank Dr. E. Runge for stimulating discussions. This work was supported by DARPA through ONR Contract No. N00014-96-1-0887 and NSF Grant No. Che9610501.

APPENDIX A

This appendix presents the detailed formulas for the Coulomb part of the dynamical matrix, derived using the Ewald procedure as described in the text of the article. Letting κ label the atoms of the SL unit cell, M_κ be the mass of the κth atom, and $\mathbf{x}(\kappa\kappa')$ be the separation vector from the κth atom to the κ'th atom, we have, for $\kappa \neq \kappa'$,

$$C^{\mathrm{Coul}}_{\alpha\beta}(\kappa\kappa'|\mathbf{k}) = -\frac{e_\kappa e_{\kappa'}}{\sqrt{M_\kappa M_{\kappa'}}} e^{i\mathbf{k}\cdot\mathbf{x}(\kappa'\kappa)} \frac{\partial^2 \phi(\mathbf{k},\mathbf{r})}{\partial r_\alpha \partial r_\beta}\bigg|_{\mathbf{r}=\mathbf{x}(\kappa'\kappa)}, \tag{A1}$$

where $\phi(\mathbf{k},\mathbf{r})$ is by definition

$$\phi(\mathbf{k},\mathbf{r}) = \sum_l \frac{e^{i\mathbf{k}\cdot\mathbf{x}(l)}}{|\mathbf{x}(l)+\mathbf{r}|}, \tag{A2}$$

$\mathbf{x}(l)$ being the position of the lth unit cell. The result of the Ewald procedure adapted to the superlattice is that $\phi(\mathbf{k},\mathbf{r})$ can be written in the form

$$\begin{aligned}\phi(\mathbf{k},\mathbf{r}) = {} & R\sum_l H(|\mathbf{x}(l)+\mathbf{r}|R) e^{i\mathbf{k}\cdot\mathbf{x}(l)} \\ & + \frac{2\sqrt{\pi}}{v_\parallel} \sum_{h_\parallel, l_z} \frac{2}{|\tau(h_\parallel)+\mathbf{k}_\parallel|} \\ & \times I\left(\infty, \frac{|\tau(h_\parallel)+\mathbf{k}_\parallel|}{2R}, \frac{|\tau(h_\parallel)+\mathbf{k}_\parallel||\mathbf{x}(l_z)+z|}{2}\right) \\ & \times e^{-i(\tau(h_\parallel)+\mathbf{k}_\parallel)\cdot\mathbf{r}_\parallel + ik_z\hat{z}\cdot\mathbf{x}(l_z)},\end{aligned} \tag{A3}$$

where R is an arbitrary cutoff (we always take $R = 3/a_0$),

$$H(x) = \frac{2/\sqrt{\pi}}{x}\int_x^\infty e^{-x'^2} dx', \tag{A4}$$

$v_\parallel$ is the area of the unit cell in the superlattice plane, l_z labels the layers perpendicular to the growth (z) axis, $h_\parallel = (h_x, h_y)$ labels the cells located at reciprocal lattice vectors $\tau(h_\parallel)$ in each plane, $\mathbf{k} = (\mathbf{k}_\parallel, k_z)$, and

$$I(\alpha,\beta,\gamma) = \int_\beta^\alpha e^{-v^2 - \gamma^2/v^2} dv. \tag{A5}$$

For $\kappa = \kappa'$ we have

$$\begin{aligned}C^{\mathrm{Coul}}_{\alpha\beta}(\kappa\kappa|\mathbf{k}) = \frac{e_\kappa}{M_\kappa}\Bigg[& -e_\kappa \sum_{l\neq 0} e^{i\mathbf{k}\cdot\mathbf{x}(l)} \left(\frac{\partial^2 r^{-1}}{\partial r_\alpha \partial r_\beta}\right)_{\mathbf{r}=\mathbf{x}(l)} \\ & + \sum_{l'\kappa'\neq 0\kappa} e_{\kappa'} \left(\frac{\partial^2 r^{-1}}{\partial r_\alpha \partial r_\beta}\right)_{\mathbf{r}=\mathbf{x}(l'\kappa',0\kappa)}\Bigg].\end{aligned} \tag{A6}$$

The first term on the right is similar to the above expression in Eqs. (A1)–(A3) but for the $l=0$ in Eq. (A3) term one substitutes $(4/3\sqrt{\pi})\delta_{\alpha\beta}$. The second term is given by

$$\frac{\partial^2}{\partial r_\alpha \partial r_\beta}[I_0 + I_1 + I_2]_{\mathbf{r}=0}, \tag{A7}$$

with

$$I_0 = \mathrm{Re}_\kappa H^0(|\mathbf{r}|R), \tag{A8}$$

$$I_1 = R\sum_{l'\kappa'\neq 0\kappa} e_{\kappa'} H(|\mathbf{x}(l') + \mathbf{x}(\kappa'\kappa) + \mathbf{r}|R) \tag{A9}$$

and

$$\begin{aligned}I_2 = {} & \frac{2\sqrt{\pi}}{v_\parallel} \sum_{h_\parallel, l_z, \kappa'} e_{\kappa'} \frac{2}{|\tau(h_\parallel)|} \\ & \times I\left(\infty, \frac{|\tau(h_\parallel)|}{2R}, \frac{|\tau(h_\parallel)||\mathbf{x}(l_z) + \hat{z}\cdot\mathbf{x}(\kappa'\kappa)|}{2}\right) \\ & \times e^{-i\tau(h_\parallel)\cdot(\mathbf{x}(\kappa'\kappa)+\mathbf{r})},\end{aligned} \tag{A10}$$

where

$$H^0(x) = -\frac{2/\sqrt{\pi}}{x}\int_0^x e^{-x'^2} dx'. \tag{A11}$$

A similar, but not identical, approach was used in Ref. 15.

[1] L. D. Hicks and M. S. Dresselhaus, Phys. Rev. B **47**, 12727 (1993).
[2] G. D. Mahan and L. M. Woods, Phys. Rev. Lett. **80**, 4016 (1998).
[3] G. D. Mahan, J. O. Sofo, and M. Bartkowiak, J. Appl. Phys. **83**, 4683 (1998).
[4] R. J. Radtke, H. Ehrenreich, and C. H. Grein, J. Appl. Phys. **86**, 3195 (1999).
[5] W. S. Capinski and H. J. Maris, Physica B **219**, 699 (1996).
[6] W. S. Capinski, H. J. Maris, T. Ruf, M. Cardona, K. Ploog, and D. S. Katzer, Phys. Rev. B **59**, 8105 (1999).
[7] R. Venkatasubramanian and T. Colpitts, Mater. Res. Soc. Symp. Proc. **478**, 73 (1997).
[8] R. Venkatasubramanian, E. Sivola, T. Colpitts K. Stokes, and B. O'Quinn, Mater. Res. Soc. Symp. Proc. (to be published).
[9] P. Hyldgaard and G. D. Mahan, Phys. Rev. B **56**, 10754 (1997).
[10] G. Chen, J. Heat Transfer **119**, 220 (1996); Phys. Rev. B **57**, 14958 (1998).
[11] K. Kunc, Ann. Phys. (Paris) **8**, 319 (1973–1974).
[12] K. Kunc, M. Balkanski, and M. A. Nusimovici, Phys. Rev. B **12**, 4346 (1975).
[13] S. Y. Ren and J. D. Dow, Phys. Rev. B **25**, 3750 (1982).
[14] C. Patel, T. J. Parker, H. Jamshidi, and W. F. Sherman, Phys. Status Solidi B **122**, 461 (1984).
[15] S.-F. Ren, H. Chu, and Y.-C. Chang, Phys. Rev. B **37**, 8899 (1988).
[16] M. Born and K. Huang, *Dynamical Theory of Crystal Lattices* (Oxford University Press, London, 1954), pp. 248–255.
[17] A. H. MacDonald, S. H. Vosko, and P. T. Coleridge, J. Phys. C **12**, 2991 (1979).